7 Sm-Co alloys

7.1 Introduction

The story of Sm-Co (or R-Co in general) magnet materials can be traced back to the 1940s, when the study of rare earth metals was greatly accelerated because of advances in chemical separation techniques developed in association with the Manhattan Project. Magnetic properties of $GdCo_5$ were first reported by Nesbit [1] in 1959 and Hubbard [2] in 1960. However, the significance of their work was neglected, perhaps due to the high cost of Gd and low magnetization of $GdCo_5$.

In 1966, Hoffer and Strnat [3] reported the extremely large magnetocrystalline anisotropy of YCo_5. They further predicted that YCo_5 and most other RCo_5 compounds were candidates for new high-performance magnet materials. The significance of this discovery was immediately recognized and extensive studies followed to determine the magnetic properties of RCo_5 (R = Y, Sm, Ce, La, Nd and misch metal) [4]. The preliminary YCo_5 specimen made by Strnat's group in 1966 had $(BH)_{max}$ only around 8 kJ/m^3 and in 1967, the same group reported 41 kJ/m^3 for $SmCo_5$ [5]. Further improvements in $(BH)_{max}$ for $SmCo_5$ reached 147 kJ/m^3 in 1968 by Velge and Buschow [6], and 159 kJ/m^3 by Das [7], Benz and Martin [8]. Today, the best $(BH)_{max}$ of $SmCo_5$ is around 199 kJ/m^3. Partial substitution of Pr for Sm resulted in slightly enhanced magnetization and energy product.

R_2Co_{17} compounds possess higher magnetization and Curie temperatures than RCo_5. However, it proved to be very difficult to develop useful coercivity in Sm_2Co_{17} [9-11]. It took nearly 10 years for $Sm_2(Co,Fe)_{17}$-based magnets to reach 240 kJ/m^3 by using Cu and Zr substitution for Co, coupled with a long and complex processing [12-14]. The best $(BH)_{max}$ of $Sm_2(Co,Fe,Cu,Zr)_{17}$-type magnets is 271 kJ/m^3 at room temperature.

7.2 Phase diagram and crystal structures

Figure 7-1 shows the binary Sm-Co phase diagram [15-17]. There exist quite a few intermetallic compounds in the Sm-Co system, in which $SmCo_5$ and Sm_2Co_{17} possess important technical significance. As shown in Figure 7-2, $SmCo_5$ has a hexagonal crystal structure (1:5H, space group: P6/mmm; prototype: $CaCu_5$), while Sm_2Co_{17} has a rhombohedral crystal structure (2:17R, space group: R3m; prototype: Th_2Zn_{17}) at room temperature and a hexagonal crystal structure (2:17H, space group: P63/mmc; prototype: Th_2Ni_{17}) at high temperatures (1300-1340ºC).

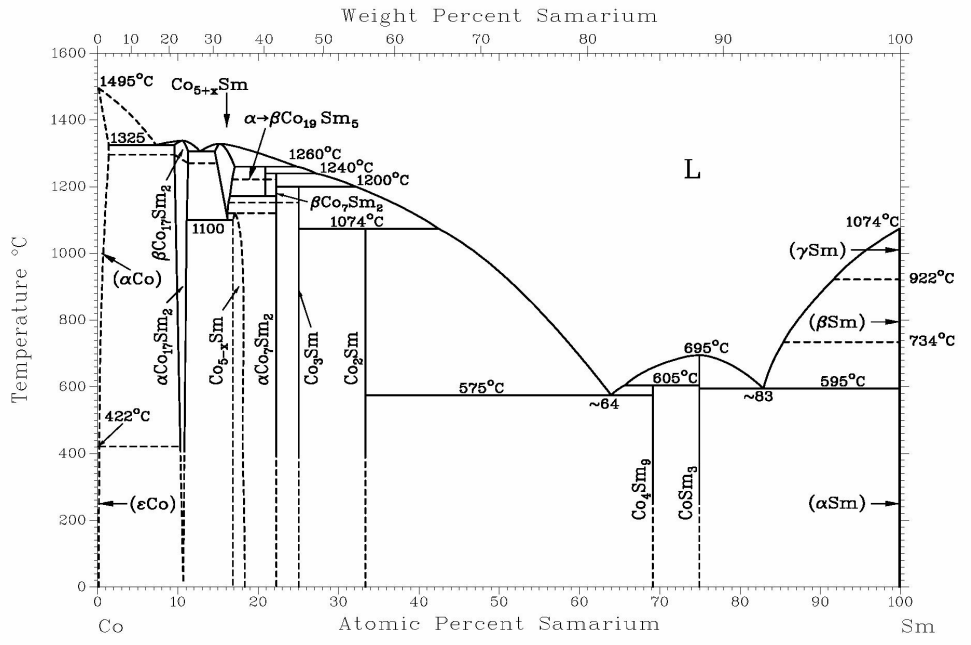

Figure 7.1 Binary Co-Sm equilibrium phase diagram.

7.3 Intrinsic properties and related compounds

Table 7.1 lists the intrinsic properties for some R-Co compounds. It is shown that of all light rare earth-Co compounds, $SmCo_5$ possesses the highest magnetocrystalline anisotropy, while Sm_2Co_{17} has the highest saturation magnetization and Curie temperature. As for heavy rare earth-Co compounds, $GdCo_5$, $TbCo_5$, $DyCo_5$, and Gd_2Co_{17} have low saturation magnetization, while Tm_2Co_{17} and Lu_2Co_{17} have rather high saturation magnetization, but with unfavorable magnetocrystalline anisotropy.

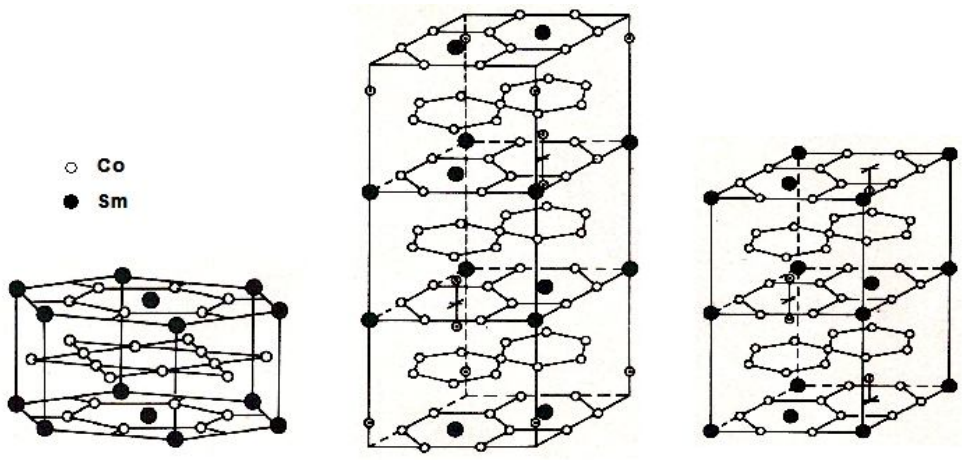

(a) 1:5 H (b) 2:17 R (c) 2:17 H

Figure 7.2 Crystal structures of $SmCo_5$ (H) (a), Sm_2Co_{17} (R) (b), and Sm_2Co_{17} (H) (c).

Table 7.1 Intrinsic properties of some R-Co compounds at room temperature.

Compound	$\mu_0 M_s$ (T)	T_C (K)	K_1 (MJ/m^3)	H_a (MA/m)	Type of anisotropy
YCo_5	1.06	987	6.5	10.3	uniaxial
$LaCo_5$	0.91	840	6.3	13.9	uniaxial
$CeCo_5$	0.77	653	6.4	16.7	uniaxial
$PrCo_5$	1.20	893	8.1	13.5	uniaxial
$NdCo_5$	1.23	910	0.7	0.4	easy basal plane
$SmCo_5$	1.07	1020	17.2	~30	uniaxial
$GdCo_5$	0.36	1008	4.6	~21	uniaxial
$TbCo_5$	0.24	980		0.5	
$DyCo_5$	0.44	966		2.0	
Y_2Co_{17}	1.25	1167	-0.34		easy basal plane
Ce_2Co_{17}	11.5	1053		1.2	easy basal plane
Pr_2Co_{17}	13.8	1171	-0.6		easy basal plane
Nd_2Co_{17}	1.39	1150	-1.1		easy basal plane
Sm_2Co_{17}	1.22	1190	3.3	5.4	uniaxial
$Sm_2(Co_{0.7}Fe_{0.3})_{17}$	14.5	1113	3.0	4.1	uniaxial
Gd_2Co_{17}	0.75	1209	-0.5		easy basal plane
Tm_2Co_{17}	12.1	1183	0.56	2.6	uniaxia
Lu_2Co_{17}	14.0	1203			easy basal plane

7.4 Permanent magnet materials

Though applications of Nd-Fe-B magnets have rapidly expanded since the mid-1980s, Sm-Co magnets are still important because of their excellent thermal stability and better corrosion resistance. Sm-Co magnets can be used at temperatures up to ~300ºC owing to their high Curie temperatures.

Sm-Co permanent magnets are based on $SmCo_5$ and Sm_2Co_{17} compounds. The composition of the $SmCo_5$ magnet is slightly Sm rich, as compared with its chemical stoichiometry. Its microstructure is basically a featherless single phase. On the other hand, the composition and microstructure of Sm_2Co_{17}-based magnets are more complicated. Figure 7.3 shows the TEM microstructure of a $Sm(Co_{0.715}Fe_{0.20}Cu_{0.06}Zr_{0.025})_{7.1}$ magnet after sintering at 1200ºC for 1 hour, followed by a solid solution heat treatment at 1180ºC for 5 hours, isothermal aging at 800ºC for 40 hours, and slow cooling from 800ºC to 400ºC at 1ºC per minute. Its intrinsic coercive force is 1,200 kA/m.

The typical microstructure of the sintered $Sm_2(Co,Fe,Cu,Zr)_{17}$-type magnet shows grains of micrometers in size, with a fine, nanometer cellular structure within each grain. As shown in Figure 7.3, the cellular structure consists of three coherent phases: a 2:17 cell interior phase; a 1:5 cell boundary phase rich in Sm and Cu; and a platelet phase rich in Zr. It is believed that the domain wall pinning in the 1:5 cell boundary phase is the origin of the high coercivity, while the high coercivity in $SmCo_5$ magnets is generally attributed to nucleation.

For most heavy rare earth-Co compounds, for example $GdCo_5$ and Gd_2Co_{17}, the magnetization increases when the temperature enhances before reaching a peak. Based on this characteristic, partial substitution of heavy rare earth, such as Gd, for Sm can be made to form a temperature-compensated (Sm,Gd)-Co magnet which may show a near zero temperature coefficient of magnetization within a temperature range.

Powder metallurgy is used to manufacture commercial Sm-Co magnets. Its processing procedures include vacuum melting, ingot crushing, ball or jet milling, powder magnetic alignment, compaction, sintering and heat treatment. Alternatively, Sm-Co alloy powders can be produced by a reduction-diffusion process, using Sm_2O_3, Co powder, and Ca or CaH_2 as a reduction agent.

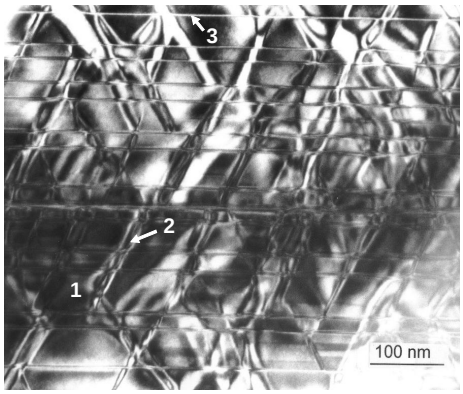

Figure 7.3 TEM micrograph of sintered a $Sm(Co,Fe,Cu,Zr)_{7.1}$ with ${}_iH_c$ = 1,200 kA/m. 1- cell interior; 2- cell boundary; 3- platelet phase.

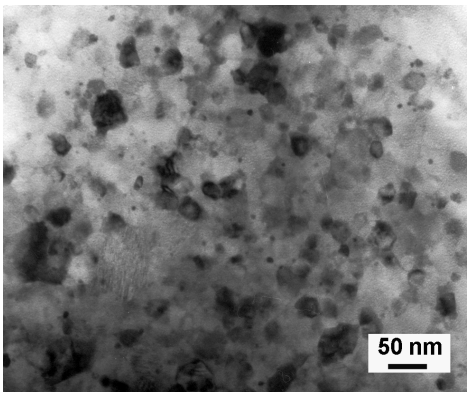

Figure 7.4 TEM micrograph of a nanograin Sm_2Co_{17} magnet sample annealed at 750ºC for 1 minute with ${}_iH_c$ = 1,240 kA/m.

Sintered Sm-Co magnets are very hard and brittle, therefore machining them into the final shape and size is often troublesome, especially for tiny magnetic parts. This led to the development of bonded Sm-Co magnets [18], which are made by consolidating a magnet powder with a polymer matrix. Thermosetting binders, such as epoxy resin, are employed for use in compression-molded magnets, while thermoplastic binders, like nylon, for injection-molded magnets, and elastomers, such as rubber, are used for extruded magnets [19]. Table 7.2 lists magnetic properties of some Sm-Co magnets.

Table 7.2 Magnetic properties of some commercial Sm-Co magnets (TM stands for Co,Fe,Cu,Zr).

Magnets	$\mu_0 M_r$ (T)	${}_M H_c$ (kA/m)	${}_B H_c$ (kA/m)	$(BH)_{max}$ (kJ/m^3)
$SmCo_5$, $(Sm,Pr)Co_5$	0.8-0.96	>1,900	635-740	135-190
Sm_2TM_{17}	1.0-1.2	>1,900	710-840	180-255
Temp. compensated $SmCo_5$	0.5-0.75	>1,900	400-600	64-120
Temp. compensated Sm_2TM_{17}	0.8-0.95	>1,900	480-720	80-175
Bonded $SmCo_5$	0.4-0.5	600-1,600	240-520	32-65
Bonded Sm_2TM_{17}	0.6-0.8	400-1,600	310-530	64-130

Demagnetization curves of commercial $SmCo_5$ and $Sm_2(Co,Fe,Cu,Zr)_{17}$-type magnets at various temperatures are shown in Figures 7.5 and 7.6 (By courtesy of Electron Energy Corporation). Both types of magnets can be used up to 300ºC. $Sm_2(Co,Fe,Cu,Zr)_{17}$-type magnets capable of operating at up to 550ºC are also commercially available; however, because of excessive additions of Cu and Zr, their room-temperature properties are relatively poor [20].

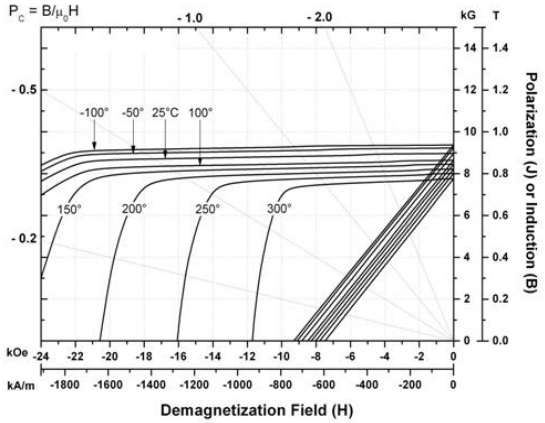

Figure 7.5 Demagnetization curves of commercial $SmCo_5$ magnets.

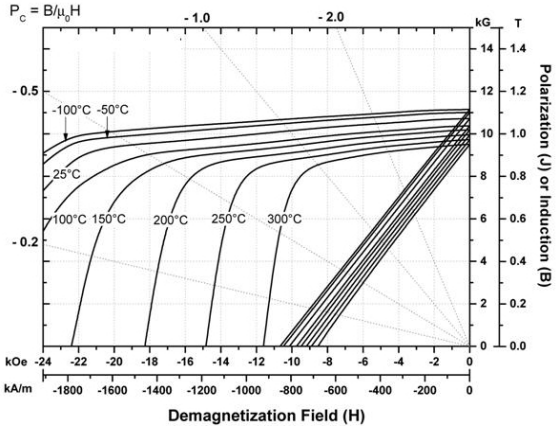

Figure 7.6 Demagnetization curves of commercial Sm_2TM_{17} magnets.

7-5 Nanograin Sm-Co magnets and significance of nanograin structure

A fundamental change takes place for the coercivity mechanism when the grain size reduces from micrometer to nanometer range. A convincing example is Sm_2Co_{17}. High coercivity can be developed in stoichiometric nanograin Sm_2Co_{17} [21,22]. Intrinsic coercivity of 1,240 kA/m was easily obtained after annealing the high-energy ball milled Sm_2Co_{17} powder at 750ºC for only 1 minute [23]. The TEM microstructure of this magnet sample is given in Figure 7.4. It should be noted that in order to achieve the similar level of coercivity, its micrograin counterpart must go through a sintering and long-term heat treatment totaling 70 hours, in addition to the Cu and Zr addition.

Therefore, high uniaxial magnetocrystalline anisotropy is not only a necessary condition for high coercivity, as it is in micrograin magnet materials, but it is also the sufficient condition for high coercivity in nanograin magnet materials. In other words, a direct connection between the high coercivity and the high anisotropy is established in nanograin magnet materials. This concept was also confirmed in YCo_5 and stoichiometric $Ne_2Fe_{14}B$ [23].

Surfactant-assisted high-energy ball milling has been used to produce anisotropic $SmCo_5$ nanoflakes, and the subsequent magnetic alignment and compaction would yield bulk, anisotropic, nanocrystalline $SmCo_5$ magnets [24-27]. Alternatively, bulk, anisotropic, nanograin $SmCo_5$ magnets with coercivity of 795-3,980 kA/m and $(BH)_{max}$ of 88-135 kJ/m^3 were synthesized by hot compacting the high-energy ball milled $SmCo_5$ powder at 700ºC, followed by hot deformation at 800-900ºC with a height reduction of 70-90% [28]. Figures 7.7 and 7.8 show microstructures of anisotropic $SmCo_5$ nanoflakes [25] and a hot-deformed bulk, anisotropic, nanocrystalline $SmCo_5$ specimen [28], respectively.

7.6 Nanocomposites and exchange spring

In a nanograin rare earth magnet material, the rare earth content can be reduced to lower than its chemical stoichiometric composition, resulting in a hard-soft nanocomposite magnet material. In nanocomposites, because of the hard/soft interface exchange coupling, the direction of magnetization in the soft phase is restricted by that in the hard phase and tends to be aligned in the same direction as that in the hard phase. The exchange interaction of magnetic moments at the hard/soft interface is, in a way, like a spring, leading to the term exchange spring.

In recent years, many processing approaches were adopted trying to make bulk, anisotropic, nanocomposite $SmCo_5$/α-Fe magnets, such as powder blending, powder particle coating, magnetic field-assisted ball milling [24-27,29], however, the magnetic performance of the new magnets are still poorer than that of conventional $SmCo_5$.

It has been nearly 30 years since Buschow's group first reported magnetic properties in hard-soft nanocomposites [30]. However, nanocomposite magnets, including both Sm-Co and Nd-Fe-B systems, remain in the laboratory research stage and their magnetic performance is still poorer than their conventional counterparts. Technical difficulties in developing practical nanocomposite magnets include not only how to make bulk, fully dense, anisotropic magnets using adequate processes, but also how to develop sufficiently high intrinsic coercivity to ensure a linear induction demagnetization curve, which is critical for all dynamic applications, such as for motors, generators, and actuators.

7.7 Thin films and epitaxy

In addition to bulk magnets, Sm-Co thin films have been used in areas including, but not limiting to, microelectromechanical systems (MEMS) and magnetic recording. MEMS are miniaturized electromechanical devices, such as motors, actuators, sensors, mini-pumps, and micro-systems with coupled electric, mechanical, radiant, thermal, magnetic, and chemical effects. Some MEMS applications require a permanent magnet film up to a few hundred nanometers in thickness, while others use a permanent magnet 'thick layer' of a few microns, some even to a few tenths of millimeters. [31].

Permanent magnets used for MEMS should have (1) proper H_c, high B_r, $(BH)_{max}$, and T_C; (2) adequate ~~to~~ MEMS processing; and (3) environmental stability, including mechanical stability, chemical stability, and thermal stability. Among all potential candidates, $SmCo_5$ thin film demonstrates the best magnetic performance; however, its corrosion resistance is poorer than that of some other materials, such as Pt-Co [31].

The perpendicular magnetic recording can provide the storage density three times more than the traditional longitudinal recording. For the perpendicular recording, a thin film possessing high uniaxial anisotropy, with its c-axis perpendicular to the substrate surface, is required. This can be accomplished by epitaxially growing $SmCo_5$ thin film on an appropriate underlayer [32].

Epitaxial $SmCo_5$ thin films with strong perpendicular magnetic anisotropy have been developed using sputtering or pulse laser deposition on various substrates, including Cu, Cu/Ti, W, Cr/Cu, Al_2O_3 (0001), heated Ru buffered Al_2O_3 (0001), Cr buffered single crystal MgO (110), and Ru/Cu/Ru sandwich, etc. and large perpendicular anisotropy and high coercivity have been achieved [32-35].

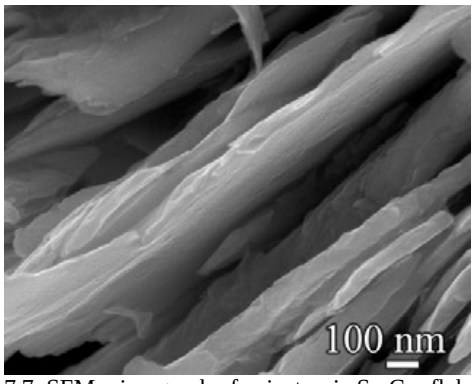

Figure 7.7 SEM micrograph of anisotropic $SmCo_5$ flakes prepared by surfactant-assisted high-energy ball milling.

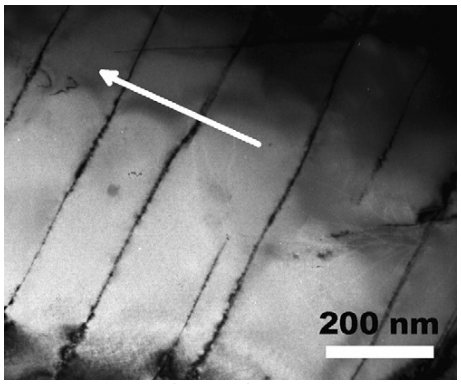

Figure 7.8 TEM graph of hot deformed $SmCo_5$ with 90% height reduction.

References

1. E.A. Nesbitt, J.H. Wernick, and E. Corenzwit, J. Appl. Phys., **30** : 365 (1959)
2. W.M. Hubbard, E.Adams, and J.V. Gilfrich, J. Appl. Phys., **31** : 3685 (1960)
3. G. Hoffer and K. Strnat, IEEE Trans. Magn. **2** : 487 (1966),
4. K.J. Strnat and G. Hoffer, Air Force Materials Lab., Technical Report AFML-TR-65-446, Dayton, Ohio (1965).
5. K. Strnat, G. Hoffer, J. Olson, W. Ostertag, and J.J. Becker, J. Appl. Phys., **38** : 1001 (1967)
6. W.A.J.J. Velge and K.H.J. Buschow, J. Appl. Phys., **39** : 1717 (1968)
7. D.K. Das, IEEE Trans. Magn. **5**: 214 (1969)
8. M.G. Benz and D.L. Martin, Appl. Phys. Lett., **17** : 176 (1970)
9. A.E. Ray and K.J. Strnat, Research and Development of Rare Earth Transition Metal Alloys as Permanent Magnet Materials, US Air Force Materials Lab. Technical Reports, 1971-1973.
10. A.E. Ray and K.J. Strnat, Proc. 7th Rare Earth Metals Conf., E.I. Savitsky (Ed.), A.A. Baikov Institute of Meals, Moscow, p. 75 (1972)
11. H.F. Mildrum, M.S. Hartings, K.J. Strnat, and J.G. Tront, AIP Conf. Proc. **10** : 618 (1973)
12. H. Senno and Tawara, IEEE Trans. Magn. **10** : 313. (1974)
13. T. Ojima, S. Tomizawa, T. Yoneyama, and T. Hori, IEEE Trans. Magn. **13** : 1317 (1977)
14. R.K. Mishra, G. Thomas, T. Yoneyama, A. Fukuno, and T. Ojima, J. Appl. Phys., **52** : 2517 (1981)
15. Moffatt, *Binary Alloy Phase Diagrams*, vol. 2, 2nd ed. T.B. Massalski (Ed.), p.1241. (1990)
16. Y. Khan, Proc. 11th Rare Earth Res. Conf. vol. II, 652 (1974)
17. K.H.J. Buschow and A.S. van der Goot, J. Less-Common Met. **14** : 323 (1968)
18. K.J. Strnat, *Rare Earth-Cobalt Permanent Magnets*, Ferromagnetic Materials, Vol.4, Edited by E.P. Wohlfarth and K.H.J. Buschow, Elservier Science Publishers B.V. p.186. (1988)
19. P. Campbell, *Permanent Magnet Materials and Their Applications*, Cambridge University Press, p. 51 (1996)
20. M.S. Walmer, C.H. Chen, M.H. Walmer, S. Liu, and G. E.Kuhl, IEEE Trans. Magn. **36** : 3376 (2000)
21. J. Wecker, M. Katter, and L. Schultz, J. Appl. Phys. **69** : 6058 (1991)
22. S.K. Chen, J.L. Tsai, and T.S. Chin, J. Appl. Phys. **79** : 5964 (1996)
23. S. Liu, Proc. 18th Int. Workshop on High Performance Magnets, p. 691 (2004)
24. Y P Wang, Y. Li, C.B. Rong and J.P. Liu, Nanotechnology **18** : 465701 (2007)
25. B.Z. Cui, W.F. Li, and G.C. Hadjipanayis, Acta Materialia **59** : 563 (2011)
26. N. Poudyal and J P. Liu, J. Phys. D: Appl. Phys. **46** : 043001 (2013)
27. D.W. Hu, M. Yue , J.H. Zuo , R. Pan , D.T. Zhang , W.Q. Liu , J.X. Zhang,Z.H. Guo , W. Li, Journal of Alloys and Compounds **538** : 173 (2012)
28. M. Yue, J. H. Zuo, W. Q. Liu, W. C. Lv, D. T. Zhang, J. X. Zhang, Z. H. Guo, and W. Li., J. Appl. Phys. **109** : 07A711 (2011)
29. Y. Shen , S.O. Leontsev , Z. Turgut , M.S. Lucas , A.O. Sheets , and J.C. Horwath, IEEE Trans. Magn, **49** : 3244 (2013)
30. K.H.J. Buschow, D.B. Dc Mooij, and R. Coehoorn, J. Less-Common Metals, **145** : 601 (1988)
31. T. Chin , J. Magn. Magn. Mat. **209** :75 (2000)
32. A. Morisako, I. Kato, S. Takei, X. Liu, J. Magn. Magn. Mat. **303** : 274 (2006)
33. J. Sayama, K. Mizutani, T. Asahi, J. Ariake, K. Ouchi, T. Osaka, J. Magn. Magn. Mat. **301** : 271 (2006)
34. J. Sayama, K. Mizutani, T. Asahi, and T. Osaka, Appl. Phys. Lett. **85** : 5640 (2004)
35. M. Ohtakea, Y. Nukagaa, F. Kirinob, M. Futamotoa, J. Crystal Growth, **311** : 2251 (2009)

Acknowledgement

The author would like to thank Prof. D.T. Zhang of Beijing University of Technology, Y. Shen of University of Dayton, Dr. J. F. Liu of Electron Energy Corporation, Prof. J. Edmondson of Michigan State University, Lucia Liu of Georgia Institute of Technology, and J.P. Liu of University of Texas at Arlington for their help in preparing this manuscript.